Academic Journal of Science and Technology
ISSN: 2771-3032 | Vol. 7, No. 3, 2023

Design of Dual-tiltable Ducted-Fan Aircraft Based on Cross-coupling Network Control

Xinchao Liu, Zeqing Chen, Ronghao Guo

School of Electronics and Information Engineering, Xi'an Technological University, Xi'an 710021, China

Abstract: In recent years, with the rapid development of drone technology, unmanned aerial systems have been widely applied in various fields. Although the flight control and airframe structure of traditional multirotor aircraft are fairly mature, they still face challenges such as low aerodynamic efficiency, low safety, and complex structure. In order to solve these issues, a dual-tiltable-ducted-fan aircraft system is designed. The system is equipped with an STM32F407 processor as the main controller, which receives motion control information from the remote control module. By employing cross-coupling network control methods, it coordinates the output values and tilt angles of the two channeling fans to achieve stable control of the aircraft's flight attitude.

Keywords: Cross-coupling network, Tilt angle, Ducted fan, Aircraft.

1. Introduction

Unlike common quad-copters or hexa-copters, traditional unmanned aircraft have limited response speed and agility in flight due to their fixed-angle rotors, which can only change the aircraft's attitude and motion through rotor power output methods. The power of the vectored thrust dual-rotor aircraft is weak, and the efficiency of the only double-ducted fan aircraft that exists is also relatively low since the ducts are at a fixed angle and can only be controlled by grid fins or planar fins. Dual-tiltable-ducted-fan aircraft combines the advantages of tilt-wing and ducted fan, allowing it to maintain high agility while achieving high thrust. This makes it particularly suitable for military applications with special requirements. However, this type of aircraft has multiple control axes and a complex model, making it difficult to deploy conventional closed-loop control systems. By utilizing cross-coupling control methods and transforming it into a networked control structure, the control logic can be simplified, leading to improved control effectiveness.

Whether it is single-axis control or multi-axis control, the control objective is to eliminate the error between the actual position and the commanded position of each individual motion axis, for example, the tracking error of each independent motion axis. If only the error of a single axis is controlled without considering the errors and motion conditions of other motion axes, significant trajectory errors may occur, especially during high-speed movements or when there are differences in parameters among the motion axes. To solve these issues, the approach used in this study is for each individual axis's position controller to receive not only the error and motion information from its own axis but also the error and motion information from other motion axes. This allows the motion control of each axis to be coordinated with the motion control of other axes, forming the basic idea of multi-axis cross-coupling network control.

2. Analysis of the Mechanical Model of the Dual-tiltable-ducted-fan Aircraft

In order to study the control methods of the double-pendulum channeling aircraft, it is necessary to construct the mechanical model of the aircraft and analyze it, in order to establish the model framework that serves as the basis for system research.

Figure 1 shows the force situation of the dual-tiltable-ducted-fan aircraft which has different motion states in the case of ideal conditions. Symbol f1 and f2 represent the lift provided by the left and right electric ducts, respectively, where fi = bω2i (b>0, i=1,2). Q1 and Q2 are the reverse torques generated by the rotation of the left and right electric ducts, respectively. Pithθ, Rollφ, and YawΨ represent the pitch angle, roll angle, and yaw angle of the aircraft, respectively. spinβ1 and spinβ2 are the rotation angles provided by the servo systems on the right and left sides, respectively. e1, e2, and e3 are unit vectors along the ex-axis, ey-axis, and ez-axis, respectively.

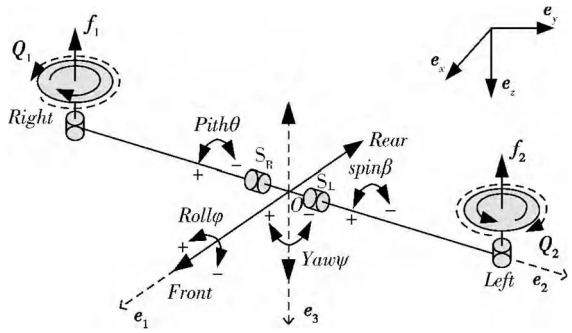

Figure 1. Force situation of the dual-tiltable-ducted-fan aircraft in the case of ideal conditions.

Figure 2 shows a schematic of the force situation in the case of various typical flight attitudes of the dual-tiltable-ducted-fan aircraft. Based on Figure 1, L1 represents the distance from the center of gravity O to the axis O1 of the right motor, and L2 represents the distance from the center of gravity O to the axis O2 of the left motor. β1 is the angle of rotation of the right arm controlled by the servo motion control system on the right, and β2 is the angle of rotation of the left arm controlled by the servo motion control system on the left.

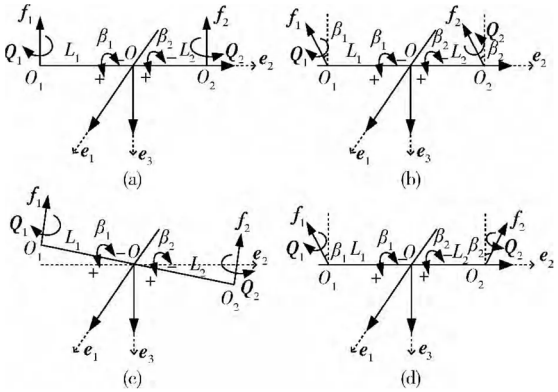

Figure 2. Schematic of the force situation in the case of various typical flight attitudes of the dual-tiltable-ducted-fan aircraft

3. Design and Implementation of the Experimental Prototype of the dual-tiltable-ducted-fan aircraft

3.1. Design of the Aircraft Prototype

The mechanical structure design of the aircraft is a necessary prerequisite for flight. The aircraft prototype must have the basic ability to adjust pitch, roll, and yaw in its mechanical structure. At the same time, while possessing these capabilities, the structure should also be sufficiently simple. As Figure 3 shows, ① Aircraft rack ②Ducted-fan ③Tilting mechanism ④Crossbeam⑤Titling gear⑥Servo motor⑦Supports of ducted-fan.

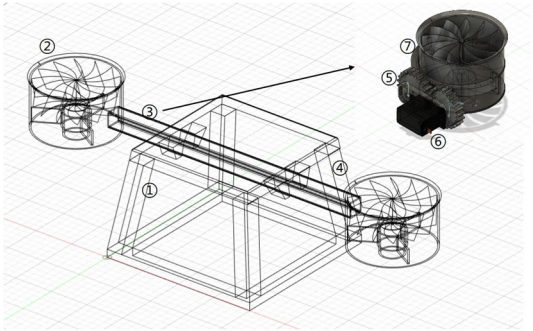

Figure 3. Mechanical structure design of the dual-tiltable-ducted-fan aircraft

A payload module for the unmanned aerial vehicle (UAV) was also designed. The UAV payload module has the capability to deliver loads and contains compartments for housing power batteries. Once the power batteries are loaded, the payload module ensures that the center of gravity is below the center of lift, providing static stability. Furthermore, the payload capacity of the module does not compromise the system stability; instead, it enhances its resistance to disturbances.

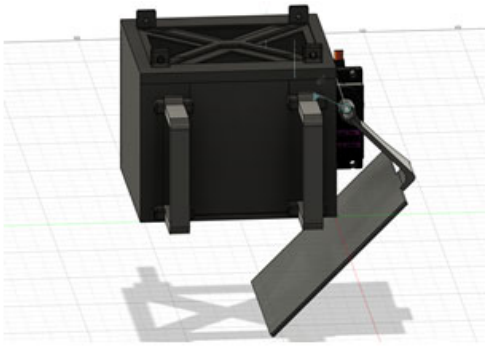

Figure 4. Mechanical structure design of the payload module

3.2. Hardware of the control system

3.2.1. Main controller: STM32F407

The STM32F407 is a microcontroller based on the ARM Cortex-M4 core, manufactured by STMicroelectronics, a European semiconductor company. It is one of the highest-performing products in the STM32 series of microcontrollers. Its clock speed can reach up to 168 MHz (capable of achieving a running speed of 210 DMIPS), greatly improving its ability to perform floating-point operations or DSP processing. The STM32F4 has features such as high performance, low power consumption, and rich peripheral interfaces, making it suitable for a wide range of applications.

Figure 5. STM32F407 micro controller

3.2.2. Communication module: ESP01-S

The ESP01-S module is a WiFi module based on the ESP8266 chip developed by Espressif Systems. The ESP8266 is a Wi-Fi module that integrates a TCP/IP protocol stack, and users can program it using AT commands to enable WiFi connectivity and data transmission. In this case, the module will be used for WiFi transparent transmission using the TCP protocol to transmit a large amount of flight data.

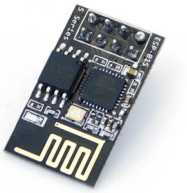

Figure 6. ESP01-S Module

3.2.3. OLED screen

This system utilizes a 0.9-inch OLED screen as the information display module. An OLED screen is a type of display screen that is made up of organic light-emitting diodes (OLEDs). It has several outstanding features, including self-emitting organic electroluminescent diodes, which eliminates the need for a backlight source. OLED screen offer high contrast, thin thickness, wide viewing angles, fast response times, and can be used on flexible panels. It also has a wide operating temperature range and a relatively simple

construction and manufacturing process.

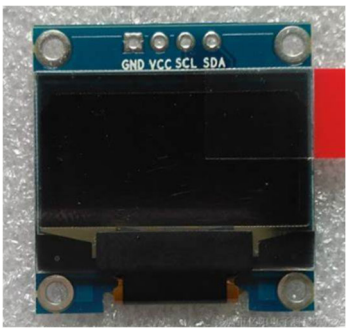

Figure 7. 0.9-inch OLED screen

3.2.4. Ducted-fan with BLDC

A ducted-fan is a power system that surrounds the fan with an annular duct. The power of the ducted fan consists of two parts: one part generated by the fan itself, and the other part generated by the annular duct. The main advantages of a ducted fan compared to an isolated fan of the same diameter are its ability to generate greater lift and the fact that the fan is enclosed within the annular duct. This design not only blocks the aerodynamic noise generated by the fan from propagating outward but also provides a compact and high level of safety, protecting the rotating blades.

Figure 8. Ducted-fan with BLDC

3.2.5. Brushless ESC

A brushless ESC (Electronic Speed Controller) refers to an electronic device used to control brushless motors. Its main function is to adjust the motor's speed and direction, allowing it to adapt to various working requirements. During the operation of a brushless motor, the ESC can detect the motor's speed and load conditions. By controlling the current and voltage, it achieves precise speed regulation and control. The ESC used in this system utilizes PWM (Pulse Width Modulation) for control.

Figure 9. Brushless ESC

3.2.6. Digital Servo Motor

This system utilizes the ES3054 metal gear digital servo, which can rotate within a range of 0 to 60 degrees and provides a maximum torque output of 3.5Kgfcm. With this servo, the desired tilt function can be achieved. This servo consists of a motor, reduction gears, control circuitry, and more. It only requires sending a single PWM signal to maintain a specified position. It also has a microprocessor that performs certain processing on the input signal based on the set parameters before delivering power pulses to the motor. Additionally, it offers higher positional accuracy, allowing for better fulfillment of tilt requirements.

Figure 10. Digital servo motor

3.2.7. MPU9250

The MPU9250 is a composite chip packaged in an OFN (Oplow-Profile Fine Pitch No-Lead) package, consisting of two parts. One part is a 3-axis accelerometer and a 3-axis gyroscope, while the other part is the AK8963 3-axis magnetometer from AKM company. Therefore, the MPU9250 is a 9-axis motion tracking device. The focus of the design in this system lies in the closed-loop control of the attitude or posture.

Figure 11. MPU9250 motion sensor module

3.2.8. S-BUS remote control module

In aeromodelling control, common remote control methods include PWM control, DSHOT, SBUS, etc. In this design, to increase stability, a digital communication protocol-based S-BUS remote control module was selected. Since data packets are utilized, environmental interference problems can be greatly reduced, ensuring the accuracy of remote control data.

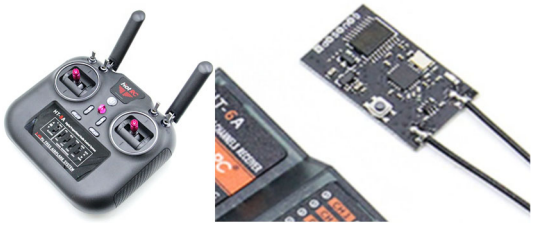

Figure 12. S-BUS remote controller and receiver

3.3. Control system software design

In terms of program design, due to the networked control and high coupling, there are multiple concurrent real-time tasks. To address this issue, the open-source and free FreeRTOS operating system was used.

During system startup, all subprocesses first wait for the initialization process to complete. Once initialization is finished, the system has access to valid initialization data, and the initialization program terminates itself. After the program begins executing concurrent tasks, there is only coupling between the filter and MPU data conversion tasks. Therefore, the filter blocks the MPU task before execution to ensure that the data is from the same sampling time point. After the data

filtering and conversion are completed, the MPU task is then enabled, and this cycle continues. Within this cycle, the interval between each iteration can be freely set to obtain a suitable and stable data flow. The program framework is illustrated in figure 13.

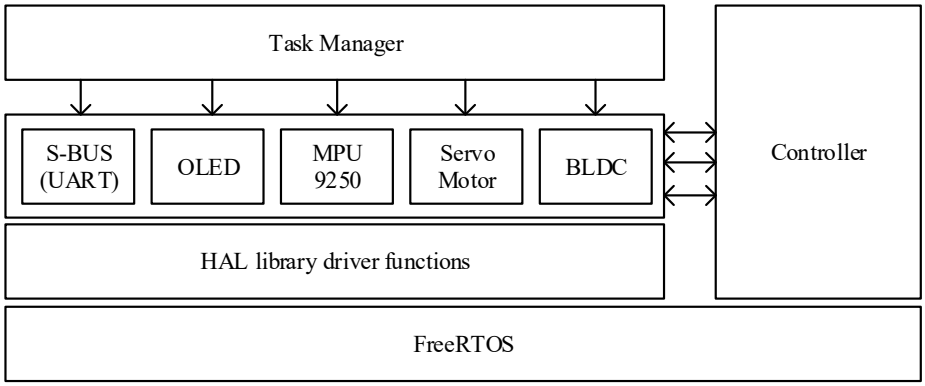

Figure 13. Program framework based on FreeRTOS kernel

After obtaining the latest control data output, the controller can internally add up the output values of multiple channels in proportion. The summed value is finally sent to two servos and two ducted fans. Before sending, the system does not correct the attitude. Since attitude data is obtained serially, it has a certain delay and phase difference. If the attitude data is still not blocked and directly injected into the control loop, it may cause confusion and coupling errors in the system. Therefore, the data is packaged in a blocking manner and injected into the loop in a time-sliced manner. This sacrifices some immediacy to ensure a unified and organized data flow. When dividing the weights internally, the conventional double-closed loop approach (stable loop and motion loop) is still used. Firstly, the basic control quantity for self-stabilization is formed for convergence. The motion loop is added before the stable loop as a sub-loop, and the motion loop does not affect the convergence effect of the stable loop when it is not enabled or no external disturbances have been introduced.

4. Verification and Analysis

4.1. Introduction to test environment

To ensure the safety of testing experiments, the aircraft is suspended on a test rig for parameter measurements during the tests. In order to facilitate the testing process, a debugging data interface was reserved in the system design to transmit flight attitude data to the upper computer. It can also receive real-time test parameters sent from the upper computer, in order to do the dynamic testing.

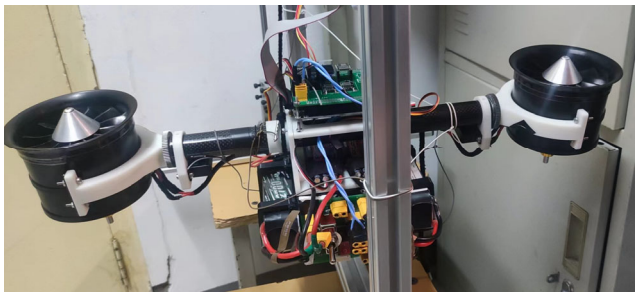

Figure 14. Dual-tiltable-ducted-fan aircraft on the test rig

4.2. Verification of YAW loop convergence test

During the convergence control experiment of the YAW loop, an incremental PID controller is used. Due to the lack of a clear system transfer function description in the manufacturing process of the aircraft, a trial-and-error method is used to tune and debug the PID parameters, and the debugging data interface mentioned above is used to record data. The following table shows some test parameters during the PID parameter tuning and debugging process. Due to the tedious measurement process and the large amount of data, only a portion of the data is selected for demonstration. The table lists three sets of test parameters: a, b, and c, representing the initial, middle, and final stages of parameter tuning. It also includes the number of oscillations and convergence time of the system under these parameter conditions, facilitating comparative analysis.

Table 1. Data for PID Parameter Tuning and Debugging Process in YAW Loop (Partial)

Sets	KP	KI	KD	Number of oscillations	Convergence time (ms)
a	8.0	0	0	--	--
b	3.0	0	0	4	2070
c	0.71	0	0	0	620

By using the debugging data interface, the desired value, output value, and actual value are obtained and plotted on a graph. The green line represents the difference between the desired value and the actual value, the red line represents the PID output adjustment value, and the blue line represents the actual deviation angle. The actual test data curve is shown in Figure 15.

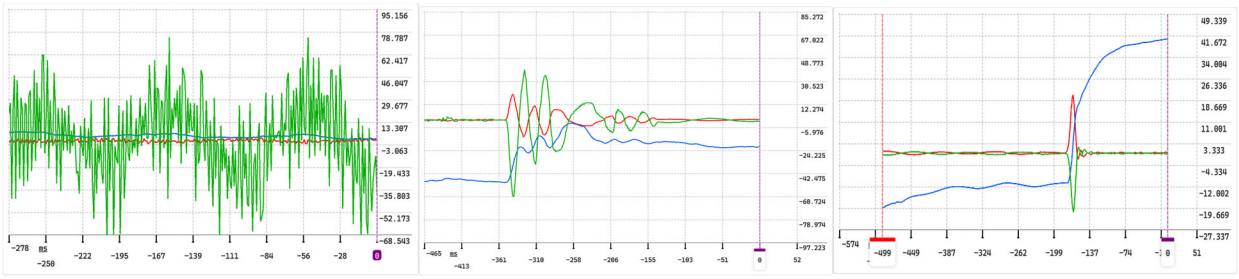

(a) (b) (c)

Figure 15. Curve plot of PID Parameter Tuning and Debugging Process in YAW Loop

During the experiment, it was found that the system had achieved good convergence characteristics without adding KI and KD values. A preliminary analysis suggests that the long arm span of the aircraft and the high inertial mass of the engine provided some damping value to the system. In addition, the mechanical structure design aims to converge the center as close as possible to the central position, minimizing the eccentricity of the YAW axis rotation action, making it easier to achieve self-stabilization.

4.3. Verification of ROLL loop convergence test

Based on the convergence of the YAW loop described above, the tuning of the ROLL loop is carried out. The convergence tuning process of the ROLL loop is similar to that of the YAW loop, but different from the angular velocity quantity of self-rotation in the YAW loop, there is a coupling relationship between the ROLL loop and gravity. Therefore, if only the steady-state angular velocity of the ROLL loop is ensured, the UAV cannot guarantee stability in the air. Therefore, in this loop, axial acceleration and Euler angle data fusion need to be added.

The following table presents the PID parameter tuning data for the ROLL loop. Five sets of PID parameters were selected during the early stage, middle stage, and final stage of parameter tuning. The number of oscillations and convergence time are provided for each set of PID parameters, allowing for a comparison of their performance.

Table 2. PID Parameter Tuning Data for ROLL Loop

Sets	KP	KI	KD	Number of oscillations	Convergence time (ms)
a	6	0	0	--	--
b	3	0	2	7	1500
c	3	0	3	--	--
d	5	0	3	--	--
e	5	1	3	4	1000

Similarly, the following graph shows the tuning data of the selected five sets of PID parameters for the ROLL loop through plotted curves. The green line represents the expected value, while the red line represents the actual attitude value.

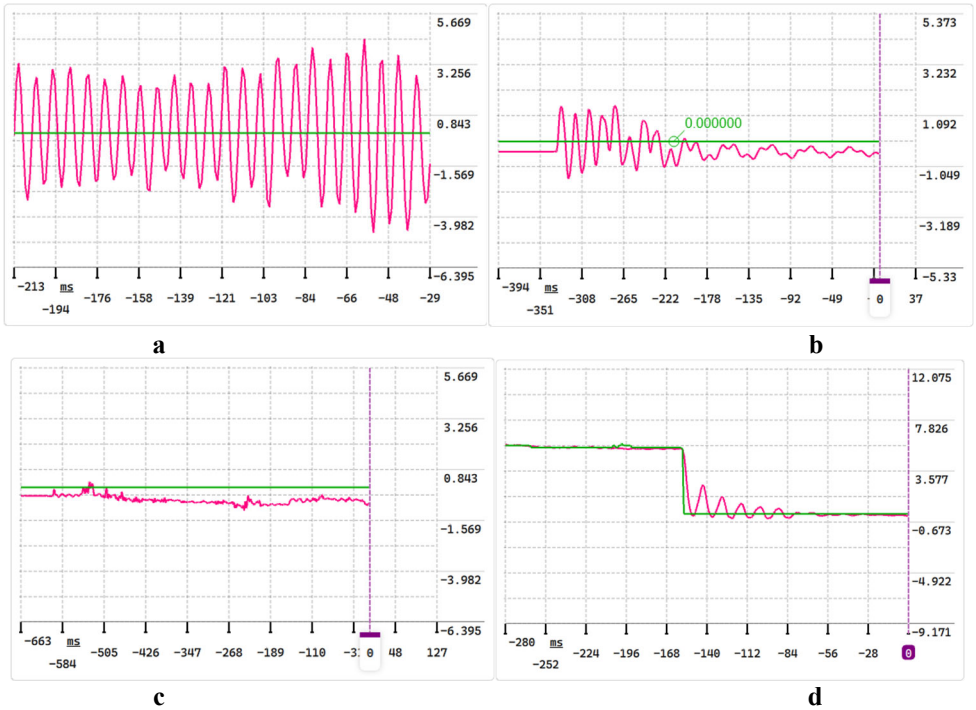

a b c d

Figure 15. Curve plot of PID Parameter Tuning and Debugging Process in ROLL Loop

Through the tuning and testing of PID parameters, the stability of the ROLL axis has reached the expected state. However, the convergence curve is not in an ideal state. An analysis shows that this is due to the change in the actual mass distribution of the aircraft caused by the revised measures for fixing the frame. This has resulted in a shift in the lower and upper limits of the oscillation curve position shown in Figure d. The measured parameters cannot be used as the actual parameters.

5. Conclusion

After multiple adjustments of the system parameters, we finally achieved a relatively stable flight effect. The system can respond to input signals in real time, and there is coupling between the two controlled loops. For example, when sending a left-rotation instruction, the thrust of the flaps will be increased as they deflect to compensate for the decrease in upward thrust caused by the tilt, while maintaining stability of the ROLL axis. However, the response speed of the ROLL axis did not reach the expected level, and there is significant lag in its response. In addition, during the experiment, the system experienced process lagging. Moreover, since the turning transmission mechanism of the aircraft was manually made, both the machining accuracy and assembly precision were not ideal. Coupled with limited testing conditions, the actual control effect still exhibits noticeable vibrations. If the machining accuracy and structural design of the aircraft can be improved, it is expected to greatly improve its controllability.

Acknowledgment

This work is supported by National Undergraduate Innovation and Entrepreneurship Training Project of China (202210702060).

References

[1] Liu, C. Design and Implementation of Dual Ducted Fan VTOL Aircraft. South China University of Technology, 2015.

[2] Zhang, F. Research and Design of Dual PMSM Speed Synchronization Control System. [Published on October 14, 2023].

[3] Chen, S., Hua, R., & Ji, B. Modeling and System Studies of Dual Ducted Tilt VTOL Aircraft. Aerospace Control, 2017, 35(1): 6. DOI: CNKI:SUN:HTKZ.0.2017-01-006.

[4] Chen, F. Control Study on the High-Speed-to-Hover Transition Flight Process of Ducted Fan Aircraft. South China University of Technology, 2021.

[5] Cong, S., & Liu, Y. Cross-Coupling Control in Multi-Axis Coordinated Motion. Machinery Design and Manufacturing, 2006(10): 3. DOI: 10.3969/j.issn.1001-3997.2006.10.069.